PCCP

Accepted Manuscript

ROYAL SOCIETY OF CHEMISTRY

www.rsc.org/pccp

Performance Improvement of Li-Rich Layer-Structured $Li_{1.2}Mn_{0.54}Ni_{0.13}Co_{0.13}O_2$ by Integration with Spinel $LiNi_{0.5}Mn_{1.5}O_4$

Xin Feng,[a] Zhenzhong Yang,[a] Daichun Tang,[a] Qingyu Kong,[b] Lin Gu,[a] Zhaoxiang Wang,*[a] and Liquan Chen[a]

Received (in XXX, XXX) Xth XXXXXXXXX 20XX, Accepted Xth XXXXXXXXX 20XX
DOI: 10.1039/b000000x

Abstract

Li-rich layered $Li_{1+x}Mn_yM_{1-x-y}O_2$ (or denoted as $xLi_2MnO_3\cdot(1-x)LiMO_2$, M = Ni, Co, Mn, etc.) are promising cathode materials for high energy-density Li-ion batteries. However, their commercial applications suffer from problems such as drops of capacity and discharge voltage during cycling. In this work, the cycling performance of layered oxide $Li_{1.2}Ni_{0.13}Co_{0.13}Mn_{0.54}O_2$ is improved by integration with spinel $LiNi_{0.5}Mn_{1.5}O_4$ to obtain a layered/spinel composite. Characterization by powder X-ray diffraction (XRD), high resolution transmission electron microscopy (HRTEM) as well as cyclic voltammetry (CV) indicates that delayed degradation of layered Li_2MnO_3 and the suppressed growth of $LiMn_2O_4$-like spinel are responsible for the performance improvement.

1. Introduction

Lithium-ion batteries have been regarded as one of the most promising power sources for portable electronic devices and electric vehicles. Exploration of cathode materials with higher energy-densities and longer cycle life is among the most important work in this field.[1] In recent years, Li-rich Mn-based oxides $Li_{1+x}Mn_yM_{1-x-y}O_2$ (M = Ni, Co, Mn, *etc*.), also known as $xLi_2MnO_3\cdot(1-x)LiMO_2$, are attractive cathode materials because of their high capacity (over 250 mAh g^{-1}) and energy density.[2,3] However, these materials suffer from drawbacks including large irreversible capacity loss in the first cycle, and capacity and discharge voltage fading in the subsequent cycles.[3,4] Much attention has been devoted to the understanding of the mechanisms for their performance decays.[3-5] Continuous transformation from the layered structure to spinel phase during cycling is generally believed responsible for the performance degradation.[6-10]

Efforts have been taken to improve the electrochemical performance of these $Li_{1+x}Mn_yM_{1-x-y}O_2$. Element doping is effective in enhancing the Li-ion conductivity and stabilizing the structure of these oxides. Substitutions such as Ru,[11] Ti,[12] Mg,[6] Cr,[13] Al,[14] *etc*. for transition metal ions (TM = Ni, Mn, and Co) and F,[14] *etc*.for O reduce the irreversible capacity in the first cycle and improve the rate performance. Surface modification is another strategy of performance improvement by suppressing the surface sensitivity of the cathode materials by changing their surface chemistry. AlF_3,[16] $LiMnPO_4$,[17] Al_2O_3,[18] PPy[19] *etc*. were used as coating materials. These efforts can indeed help to increase the capacity retention of the Li-rich materials to some extent. Recently, some studies have also paied more attention to the discharge voltage fading, such as incorporation of the polyanions (PO_4^{3-}, BO_3^{3-} or BO_4^{5-}),[20-21] application of a nonflammable electrolyte.[22] However, nor has the layer-to-spinel transformation been prevented.

Spinel $LiNi_{0.5}Mn_{1.5}O_4$ has attracted much attention in recent years because it can be charged to around 5.0 V and show good cycling stability at room temperature. In addition, its 3D Li^+ ion diffusion channels ensure its excellent rate performance.[23] More important is its structural compatibility with the close-packed oxygen array in the above Li-rich layered oxides.[24] These make the spinel material an ideal candidate to integrate with the layered oxides. Actually, layered/spinel composites such as $(0.5Li_2MnO_3{\cdot}0.5LiMn_{0.5}Ni_{0.5}O_2)$-$LiNi_{0.5}Mn_{1.5}O_4$[25] and Li_2MnO_3-$LiMn_2O_4$,[26] have been prepared to overcome some of the drawbacks of the layered and the spinel materials while retain the advantages of each. However, high content of spinel means decrease of the capacity and energy density of the composite. In addition, the interactions between the layered and spinel phases in the composites have not been considered in those reports.

In this study, Li-rich layered oxide $Li_{1.2}Ni_{0.13}Co_{0.13}Mn_{0.54}O_2$ was integrated with low content (10 wt%) of spinel $LiNi_{0.5}Mn_{1.5}O_4$ (LNMO) to suppress the voltage fading of $Li_{1.2}Ni_{0.13}Co_{0.13}Mn_{0.54}O_2$ and improve its capacity retention. Samples containing up to 50 wt% LNMO were also prepared and evaluated in order to find out the interactions between the spinel and the Li-rich layered material during material preparation and electrochemical cycling. It will be seen that the integrated spinel phase plays an important role in stabilizing the structure of its layered partner.

2. Experimental

Materials synthesis

Li-rich layered oxide material $Li_{1.2}Ni_{0.13}Co_{0.13}Mn_{0.54}O_2$ was synthesized by a modified Pechini method. Stoichiometric amounts of $Ni(CH_3COO)_2{\cdot}4H_2O$, $Co(CH_3COO)_2{\cdot}4H_2O$, $Mn(CH_3COO)_2{\cdot}4H_2O$, and excess amount

(5% in molar ratio) of $LiCH_3COO \cdot H_2O$ were used as raw materials together with citric acid and ethylene glycol (molar ratio=1:4) to form polymeric precursor. More details can be found in our previous paper.[19] The precursor was heated at 400 °C for 5 h before it was calcined at 800 °C for 12 h in air. Pure $Li_{1.2}Ni_{0.13}Co_{0.13}Mn_{0.54}O_2$ (denoted as NCM-00) was obtained after the muffler furnace was cooled down to room temperature.

Spinel-integrated $Li_{1.2}Ni_{0.13}Co_{0.13}Mn_{0.54}O_2$ containing 10, 20 and 50 wt% LNMO were prepared by a sol-gel method. Stoichiometric amounts of $Ni(CH_3COO)_2 \cdot 4H_2O$, $Mn(CH_3COO)_2 \cdot 4H_2O$, $LiCH_3COO \cdot H_2O$ for $LiNi_{0.5}Mn_{1.5}O_4$ were dissolved in de-ionized water and mixed with the above sample NCM-00 powder to form a suspension. $NH_3 \cdot H_2O$ (AR, 25%) was added into the suspension to tune its pH value to 8. The suspension was constantly stirred for 4 h at 50 °C and then dried to gel at 80 °C. The gel was kept at 110 °C until it became brown powder. A $Li_{1.2}Ni_{0.13}Co_{0.13}Mn_{0.54}O_2$-$LiNi_{0.5}Mn_{1.5}O_4$ composite was obtained after calcination at 750 °C for 12 h under an oxygen atmosphere. The $Li_{1.2}Ni_{0.13}Co_{0.13}Mn_{0.54}O_2$ with 10 wt%, 20 wt% and 50 wt% LNMO are hereafter referred to as NCM-10, NCM-20 and NCM-50, respectively.

Structure and morphology

The crystalline structure of the materials was characterized with X-ray diffraction (XRD, Bruker D8 Advance) using Cu Kα radiation (λ =1.54056 Å). High-resolution transmission electron microscopy (HRTEM), and selected-area electron diffraction (SAED) patterns were recorded on FEI Tecnai F20 transmission electron microscope.

Electrochemical testing

The electrode sheet was prepared by mixing the active material, acetylene black and polytetrafluoroethylene (PTFE) binder at a weight ratio of 80:12:8 with ethanol as the dispersant (active material: ~2 mg). The slurry was pressed into a film. The film was cut into ϕ8 circles and dried in a vacuum oven at 120 °C for 12 h. Test cells were assembled using fresh lithium foil as the counter electrode, Celgard 2300 as the separator, and 1 mol L^{-1} $LiPF_6$ dissolved in ethylene carbonate and dimethyl carbonate (1:1 v/v) as the electrolyte in an argon-filled glove box. The cell was electrochemically cycled on LAND CT2001A battery tester between 2.0 and 4.8 V (*vs*. Li^+/Li). Cyclic voltammetry (CV) data were recorded on CH Instruments electrochemical workstation at a scan rate of 0.1 mV s^{-1} between 2.0 and 4.8 V.

3. Results and Discussions

Material Characterization

Fig. 1a shows the XRD patterns of the pure and LNMO-integrated $Li_{1.2}Ni_{0.13}Co_{0.13}Mn_{0.54}O_2$ (NCM-xx). All the main diffraction peaks of NCM-00 can be indexed to the O3-$LiCoO_2$ structure ($R\bar{3}m$ symmetry group).[27] The weak peaks between 20° and 25° are attributed to the cation ordering of the Li and transition metal atoms (TM, Ni, Mn, and Co) in the TM layers.[28] Integration with LNMO does not induce any obvious changes to the structure of $Li_{1.2}Ni_{0.13}Co_{0.13}Mn_{0.54}O_2$ (NCM-00), including its TM ion ordering. A weak diffraction appears at 18.98° in NCM-10; its position shifts to lower angles with increasing integration content of LNMO and is very close to the (111) diffraction of LNMO in NCM-50 (dashed arrow in Fig. 1b). This peak is supposed to belong to Li-insufficient spinel LNMO ($Li_{1-x}Ni_{0.5}Mn_{1.5}O_4$). The main lost lithium is believed to have migrated to the lattice of $Li_{1.2}Ni_{0.13}Co_{0.13}Mn_{0.54}O_2$. Loss of lithium from $LiNi_{0.5}Mn_{1.5}O_4$ results in the oxidation of Ni^{2+} to Ni^{3+} or Mn^{3+} to Mn^{4+}. Of course, it is difficult to recognize if the newly grown spinel is $Fd\bar{3}m$ or $P4_332$ because the XRD patterns of these two phases are very similar to each other except for some very weak peaks.[29] Nor can we exclude the possibility of Co-ion migration into LNMO. The above results indicate that a thin interface exists between the Li-rich $Li_{1.2}Ni_{0.13}Co_{0.13}Mn_{0.54}O_2$ and the integrated spinel LNMO due to cation migration.

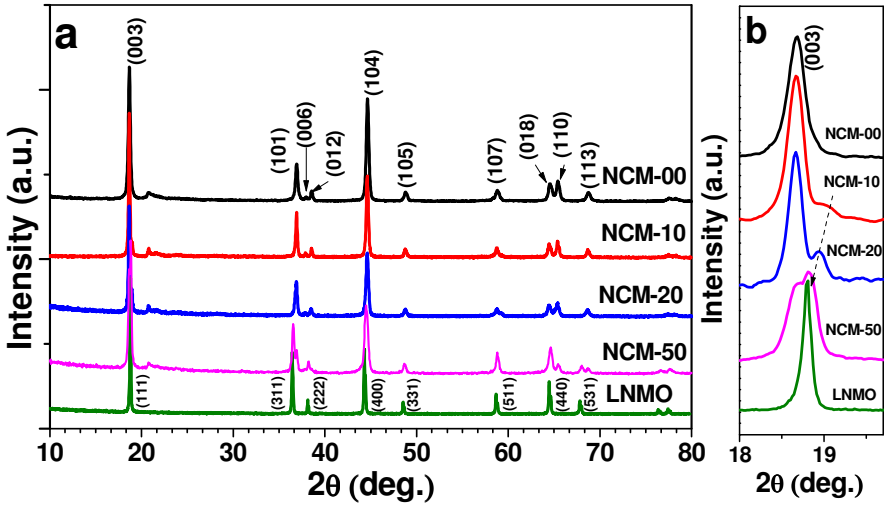

Fig. 1. Powder XRD patterns of the spinel $LiNi_{0.5}Mn_{1.5}O_4$ (LNMO)-integrated $Li_{1.2}Ni_{0.13}Co_{0.13}Mn_{0.54}O_2$. Selected XRD patterns of these samples are illustrated for showing the shifting of LNMO (111) diffraction (b).

Electrochemical Performance

Fig. 2a compares the cycling performance of $Li_{1.2}Ni_{0.13}Co_{0.13}Mn_{0.54}O_2$ integrated with various contents of LNMO. The discharge capacity of all the four samples fades fast in the first few cycles as other Li-rich cathode materials do.[9] Sample NCM-00 shows the highest reversible capacity in the beginning of cycling but its capacity retention is the poorest of the four samples. These are mainly attributed to the layer-to-spinel structural transformation.[7,8]

Integration with LNMO decreases the charge capacity of the samples due to the low cut-off charge voltage (the voltage plateau of LNMO usually finishes around 4.85 V) and the low theoretical capacity of LNMO.[29] This becomes even clearer as the content of LNMO further increases. However, the capacity of the integrated samples turns to increase after 10 to 20 cycles. After about 125 cycles, the capacity of the NCM-10 becomes higher than that of the NCM-00. The capacity retention of NCM-10 is 91.8% while that of NCM-00 is only 67.8% after 230 cycles. Increasing the content of LNMO cannot further improve the capacity retention of $Li_{1.2}Ni_{0.13}Co_{0.13}Mn_{0.54}O_2$ and decreases the discharge voltage of the composite (Fig.3d). Therefore, we do not recommend further increasing the integration content beyond 10 wt%. However, sample NCM-50 will still be used in the following discussion in order to find out why LNMO integration can improve the cycling stability of the Li-rich material.

The first charge and discharge curves of these four samples are presented in Fig. 2b. All the samples exhibit a long potential plateau above 4.5 V in the first charge, characteristic of the Li-rich layered cathode materials.[24] No traces of charge or discharge plateaus of LNMO can be observed for the 10%- and 20%-LNMO integrated samples above 4.5 V due to the low content of integration and the severe cation migration. However, short charge (*ca.* 35 mAh g^{-1}) and discharge (*ca.* 30 mAh g^{-1}) voltage plateaus can be clearly observed above 4.5 V in NCM-50. The large irreversible capacity in the first cycle is mainly ascribed to the irreversible oxygen evolution upon Li-ion extraction above 4.5 V from the Li-rich layered phase.[30]

The NCM-50 sample shows a discharge plateau at ~2.7 V. This plateau is the contribution of Li-ion insertion in the empty 16c octahedral sites, resulting in the reduction of Mn^{4+} to Mn^{3+} with a cubic-to-tetragonal phase transition of LNMO.[31,32] In contrast, NCM-10 and NCM-20 only have discharge plateaus around 2.6 V. The slight difference of the discharge plateau implies the more obvious structural modulation due to cation (not limited to Li^+ ion alone) migration and formation of non-stoichiometric LNMO upon calcination. It gets longer with increasing content of integrated LNMO, roughly in direct proportion to the LNMO content in the sample (9 mAh g^{-1} for NCM-10 and 15 mAh g^{-1} for NCM-20). It becomes less obvious in NCM-10 and NCM-20 with continuous cycling. In contrast, the discharge plateau of NCM-50 (37 mAh g^{-1}) around 2.7 V is stable upon cycling (Fig. S1c).

Fig. 2c shows the coulombic efficiency of the four samples. After integrated with LNMO, the coulombic efficiency of the first cycle improved slightly (from 77.9% for NCM-00 to 79.7 %, 79.3% and 89% for NCM-10, NCM-20, NCM-50). On the other hand, the samples show similar columbic efficiencies irrespective of integrating with LNMO after several cycles. Fig. 2d shows the rate capabilities of the various samples, the sample after integrating with LNMO shows an improved rate capability, as compared with bare Li-rich material. This can be related to the improved conductivity after integrating with LNMO.

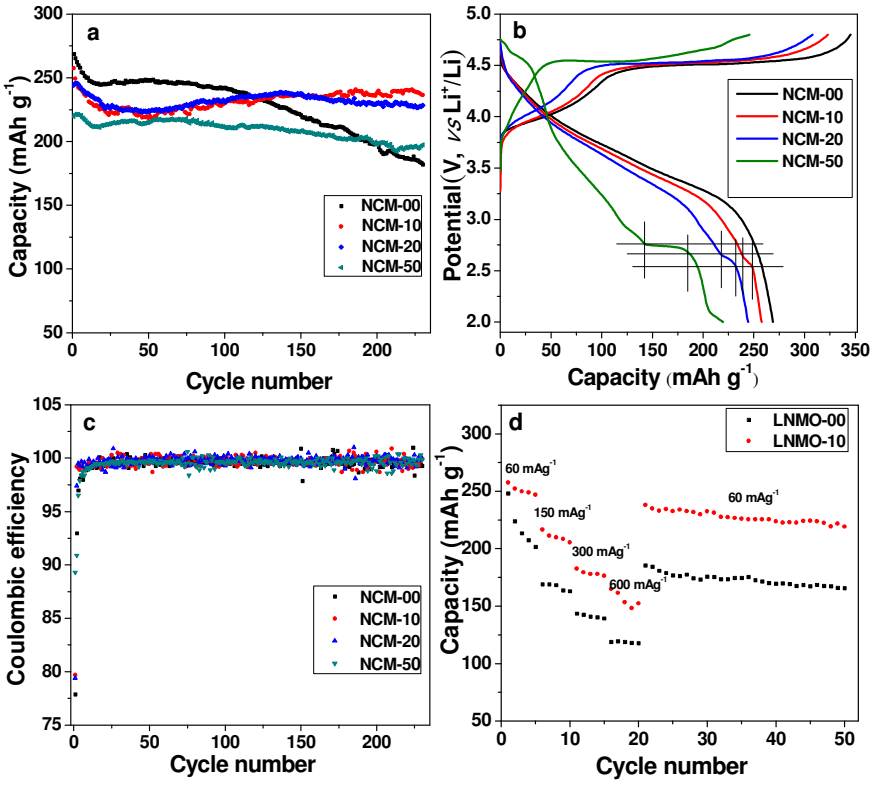

Fig. 2. The cycling performance (a), the voltage profiles in the first cycle (b), the Coulombic efficiency (c) of the cathode materials at a current density of 60 mA g^{-1} and at different current densities (d) between 2.0 and 4.8 V vs. Li^+/Li.

It has been well accepted that extensive Li^+ ion removal leads to layer-to-spinel structural transformation, responsible for the voltage instability, capacity fading, and poor rate performance of the cathodes.[2,8,33] Fig. 3a-c compare the charge/discharge profiles of NCM-00, NCM-10 and NCM-50 in the 2nd, 50th, and 200th cycles, respectively. The clear discharge voltage plateau above 4.5 V in NCM-50 contains the contribution of both LNMO and the Li-rich layered phase. The discharge plateau above 2.75 V corresponds to the spinel-like phase derived from the Li-rich phase while the plateau around 2.70 V belongs to the integrated LNMO. The shape of these plateaus does not have much change in 200 cycles in NCM-50. However, the discharge profile of NCM-00 shows no trace of the Li-rich phase above 4.5 V. These demonstrate the stabilizing effect of the LNMO integration and the stability of the integrated LNMO toward repeated cycling at low potentials. After 200 cycles, NCM-10 has the highest specific capacity and average discharge voltage, clearly indicating the stabilizing effect of LNMO integration. Moreover, the discharge midpoint potential of NCM-10 fades most slowly in all samples (Fig. 3d, the results of discharge midpoint potential were directly obtained from LAND software (CT2001A battery tester)). There is an obvious activation process between 2.8 and 4.0 V during discharge of NCM-10 and NCM-50 corresponding to the Mn^{4+}/Mn^{3+} redox reactions of Li_2MnO_3 phase in the Li-rich phase (Fig. S1). In this process,

more and more Li_2MnO_3 for lithium extraction with the removal of lattice oxygen form activated MnO_2 during charge and finally transform into $LiMn_2O_4$-like spinel.[34,35] Activation of Li_2MnO_3 leads to the increase of discharge capacity (Fig. 2a). These features become more obvious in the normalized voltage profile of these three samples after 200 cycles (Fig. S1d). That is, $LiNi_{0.5}Mn_{1.5}O_4$ integration stabilizes the structure of $Li_{1.2}Ni_{0.13}Co_{0.13}Mn_{0.54}O_2$ (actually neither is itself any longer due to cation migration; see the following).

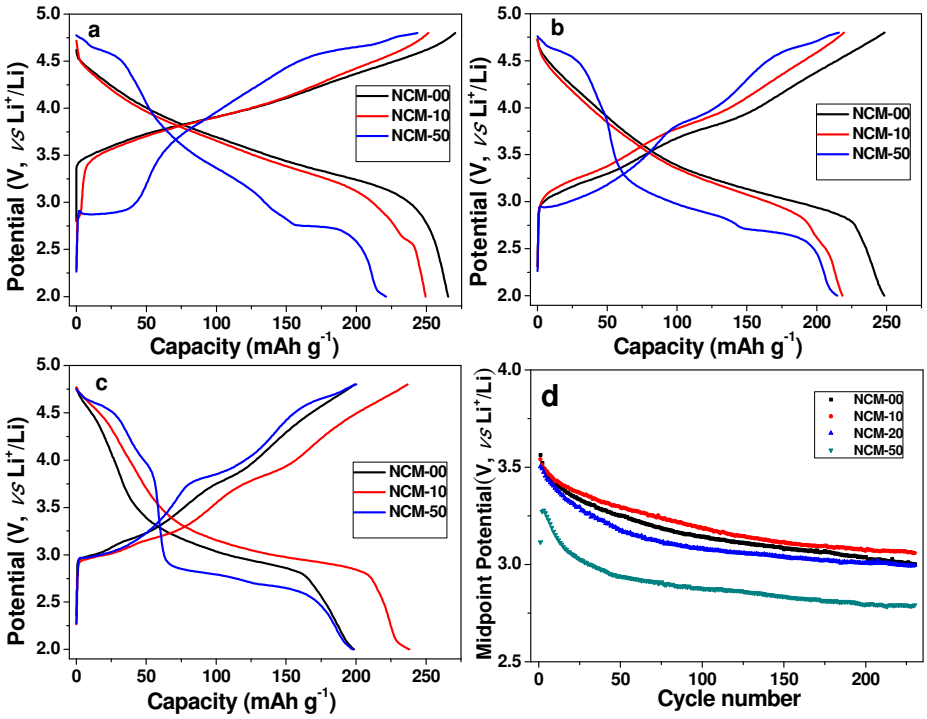

Fig. 3. Voltage profiles in the (a) 2nd, (b) 50th (c) 200th and (d) discharge midpoint potential of LNMO-integrated $Li_{1.2}Ni_{0.13}Co_{0.13}Mn_{0.54}O_2$ between 2.0 and 4.8 V vs. Li^+/Li at a current density of 60 mA g^{-1}.

Cyclic Voltammetry

The CV profiles of the NCM-00, NCM-10 and NCM-50 samples in the first three cycles were recorded between 2.0 and 4.8 V (Fig. 4a). For the anodic segment of NCM-00, the peak at *ca*. 4.0 V is attributed to the oxidation of Ni^{2+} and Co^{3+}, and the peak at *ca*. 4.6 V is associated with oxygen evolution and Li extraction from its Li_2MnO_3 component to form MnO_2.[24] Its cathodic segment is much more complicated than the anodic one. The cathodic peak at about 4.5 V is attributed to Li intercalation into tetrahedral sites in $LiMO_2$ (M = Ni, Co, Mn, *etc*.).[36,37] The reduction peak at *ca*. 3.7 V can be assigned to the reduction of Ni^{4+} and Co^{4+} in the $LiMO_2$ component of the Li-rich layered composite while the cathodic peaks around 3.6 V corresponds to the reduction of Mn^{4+} in $LiMO_2$ and MnO_2 derived from Li_2MnO_3.[38] The latter two processes are associated with the occupation of octahedral sites

by the Li^+ ions.[39,40] In the subsequent two cycles, most of the anodic/cathodic peaks shift slightly to the lower voltage. The strong anodic peak around 4.6 V almost disappears due to the irreversible Li-ion extraction and oxygen release from Li_2MnO_3.[5]

The CV profile of NCM-50 is quite different from that of NCM-00. There are 5 anodic peaks in the first charge. The peaks around 3.8 V and 4.2 V correspond to the oxidation of Ni^{2+} and Co^{3+} ions in the Li-rich layered phase and the Mn^{3+} ions in the integrated LNMO, respectively. The broad anodic peak above 4.5 V is actually composed of two peaks. The 4.62 V peak is for the oxygen evolution from the Li-rich layered phase; it is submerged in the 2nd cycle with the strong peak at 4.7 V for the oxidation of Ni^{2+}/Ni^{3+} in the integrated LNMO.[31,40] The Ni^{3+}/Ni^{4+}oxidation process is not finished here until 4.8 V. This becomes clearer in the 2nd and 3rd cycles. Usually the Ni^{2+}/Ni^{3+} and Ni^{3+}/Ni^{4+} oxidation processes are difficult to be separated due to the narrow voltage gap between them (*ca*. 20 mV) in pure spinel $LiNi_{0.5}Mn_{1.5}O_4$.[31] The clear separation of these two processes implies the doping (migration) of Co^{3+} or other ions in it during material calcination.[41] The cathodic (at 2.7 V) and anodic (at 2.9 V) peaks are attributed to Mn^{4+}/Mn^{3+} redox in LNMO.[31,32] In addition, the broad cathodic peak around 3.4 V for the reduction of Mn^{4+} in the layered phase and MnO_2 derived from Li_2MnO_3 is very weak in the 1st cycle but becomes stronger in the 2nd and 3rd cycles.[38]

With the above discussion, it is easy to understand the CV profiles of NCM-10 (Fig. 4a). The clear redox peaks below 3.0 V, about 120 mV lower than their counterparts in NCM-50, are attributed to the non-stoichiometric integrated LNMO. However, the CV of the integrated LNMO in NCM-50 is more like that of $LiNi_{0.5}Mn_{1.5}O_4$, due to the saturation of the ion migration. However, the contribution of LNMO to the CV plots of NCM-10 above 3.0 V is not obvious.

The CV profiles of NCM-00, NCM-10 and NCM-50 after 300 cycles become rather simple (Fig. 4b) in comparison with those of their first three cycles. For the convenience of discussion, the oxidation and reduction peaks of each sample are denoted as O and R peaks, respectively (the peak with the same code does not mean the same reaction in different samples). Due to the low content of the LNMO integration, the oxidation and reduction peaks in NCM-10 are mainly the contribution of $Li_{1.2}Ni_{0.13}Co_{0.13}Mn_{0.54}O_2$. The O1 peak of NCM-10 is clearly split into O1(1) and O1(2) for the oxidation of Mn^{3+} from the $LiMn_2O_4$-like spinel phase and the layered $LiM'O_2$ phase,[39,40] respectively (M′ is used here to differentiate from M because the content of the TM ions might have been changed in the layered phase after long-term cycling). However, these two peaks coalesce into one broad O1 in NCM-00. Clearly the O1 peak of NCM-10 after 300 cycles is more like that of NCM-00 after 200 cycles (Fig. S3). This difference means that the structural framework $LiM'O_2$-$LiMn_2O_4$ of NCM-10 can be better

reserved than that of NCM-00 after 300 cycles. This retention of the structural framework becomes even clearer in NCM-50. Different from those in NCM-00 and NCM-10, the O1 and R1 peaks in NCM-50 are asymmetric because they contain the contribution of the reversible cubic-to-tetragonal phase transition of the LNMO spinel phase and the $LiMn_2O_4$-like phase.[31,32]

The O2/R2 peaks indicate the redox processes of Ni and Co ions from $LiM'O_2$ layered phase and Mn ions of LNMO spinel phase.[31,40] Therefore, the R2 peak is weak in NCM-00 and NCM-10 but become stronger in NCM-50 due to contribution of the integrated spinel LNMO. In addition, its position shifts slightly to higher potentials.

The oxidation/reduction peaks for the Ni^{2+}/Ni^{3+} (O3/R3) and Ni^{3+}/Ni^{4+} (out of the recorded potential range here) of LNMO shift to higher potentials. This makes it easier to recognize the weak peak at *ca*. 4.65 V (O3 in NCM-10) for the oxidation of the O^{2-} ions. There is no such peak in NCM-00. This suggests that NCM-10 contains more Li_2MnO_3 than NCM-00 after 300 cycles. The O3 peak in NCM-50 is located at *ca*. 4.70 V. In addition, the O3 peak in NCM-10 is very broad, actually composed of the reaction of the O^{2-} ions of Li-rich phase and the Ni^{2+} ions of LNMO.

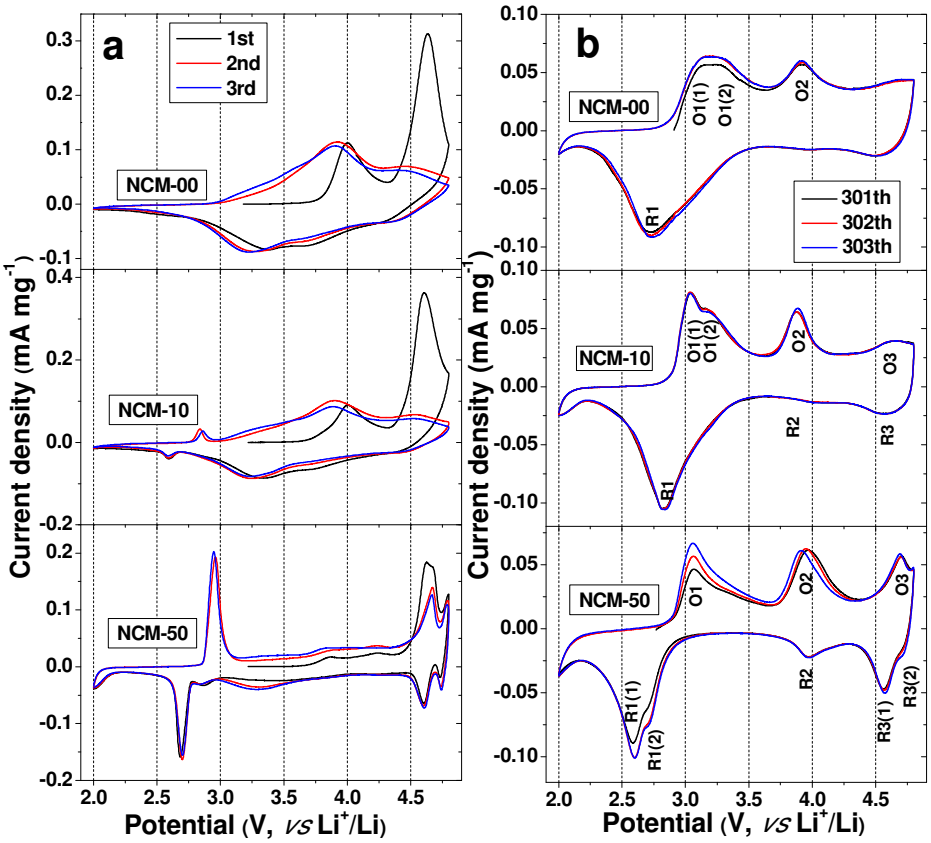

Fig. 4. The cyclic voltammograms of the first three cycles (a) and some selected cycles (b) of electrodes NCM-00, NCM-10 and NCM-50, at 0.1 mV s^{-1} between 2.0 and 4.8 V

Structural Analysis After Cycling

In order to get insight into the changes of the structure before and after long-term cycling, XRD is performed on NCM-00 and NCM-10 after 240 cycles (Fig. 5). Distinct from that of the fresh NCM-00, the diffractions of Li_2MnO_3 are absent, suggesting loss of the cation ordering in the transition metal layers.[5,38] The complicated XRD patterns are tentatively ascribed into three sets of structures, L, S1 and S2. We refer L to a layered phase $LiM'O_2$ originated from Li-rich phase but different from it in composition due to cation migration during cycling. Fig. 5 shows that all the diffraction peaks of the layered phase shift to lower 2θ angles and become broad in the NCM-00 sample. Meanwhile, their intensities are reduced or become negligible, and the adjacent peaks of (006)/(012) and (108)/(110) coalesce, respectively. With the decrease of the diffraction intensities of the L phase, a new phase as S2 is observed and becomes dominant. It is interesting that the lattice parameters of S2 are the same in both NCM-00 and NCM-10. For this reason, we believe that the S2 phase assigned to cubic spinel ($Fd\bar{3}m$) comes from the layered-to-spinel transition of the Li-rich material with continuous cycling due to the migration of TM ions and the structural rearrangement.[2,8,10] The lattice parameters of each phase are calculated and listed in Table S1. Both lattice parameters *a* and *c* increase during cycling (the result may be less reliable because the intensity of all the peaks is low and some peaks are not legible).

Different from that of the cycled NCM-00, some typical diffraction peaks indexed to layered structure still remain though diffraction peaks indexed to S1 appear in the XRD pattern of NCM-10 after 240 cycles. The S1 phase is supposed to come from the integrated spinel LNMO. However, its lattice parameter (a = 8.062 Å) is smaller than that of the integrated LNMO (a = 8.173 Å, JCPDS No. 32-0581), and its composition is also different from that of $LiNi_{0.5}Mn_{1.5}O_4$, again due to migration of both the Li and the transition metal ions during sample calcination and repeated electrochemical cycling. Although both the S1 and S2 phases are cubic, their lattice parameters, *a*, are markedly different. It is possible that the smaller Mn^{4+} ion migrates from the Li-rich phase into the LNMO spinel during cycling. Meanwhile, the larger ions such as the Ni^{2+} and Li^+ ions migrate into the lattice of the layered $LiM'O_2$ or the S2 phase from LNMO. Some earlier groups have proved that cations can migrate not only from the surface to the bulk of the particles but also from cathode to anode during the charge-discharge cycles.[3,42] Therefore, the migration of cations from one phase to another phase of cathode is possible. It seems that the quantity of the S1 phase is lower than the S2 phase, and the diffraction peaks of the S2 phase often overlap with those of the layered phase. It is the presence and growth of the S2 phase that results in the capacity and discharge voltage fading in $Li_{1.2}Ni_{0.13}Co_{0.13}Mn_{0.54}O_2$.[8] In this sense, the presence of the integrated LNMO

suppresses the growth of the S2 phase by competition. That is, the integrated S1 is like a seed; it grows by accepting some of the migrated cations. These results are consistent with the electrochemical features in the voltage profiles and the CV plots. However, they cannot explain the stabilized cycling and average discharge voltage.

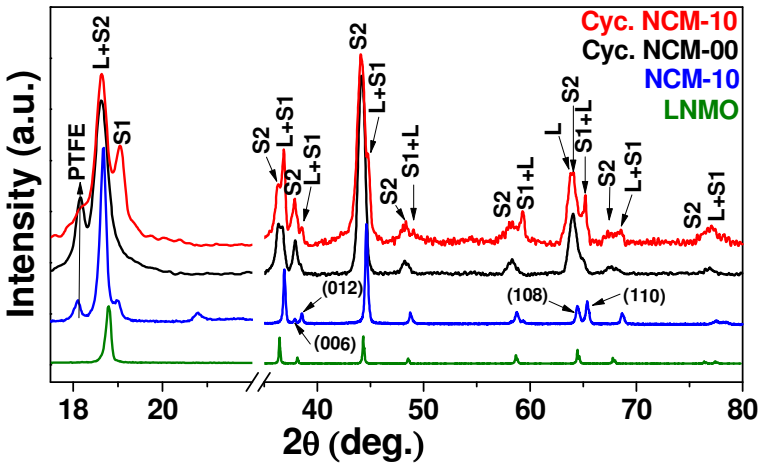

Fig. 5. XRD patterns of NCM-00 and NCM-10 electrodes after 240 cycles.

Observation of the local structure confirms the stabilizing effect of LNMO integration on the structure of the lithium-rich material. Fig. 6 compares the HRTEM and SAED images of bare and LNMO integrated $Li_{1.2}Ni_{0.13}Co_{0.13}Mn_{0.54}O_2$ samples before and after long cycles. The bare sample (Fig. 6a) shows homogeneous crystal structure from the bulk to surface before electrochemical reaction, with the d-spacing ~0.47 nm, which is close to the d-spacing of the (003) plane of R-3m structure. However, the LNMO-integrated sample (Fig. 6b) shows much different surface structure from its bulk. The d-spacing of the surface region indicated by the white arrow is about 0.236 nm, which is likely related to the (222) plane of spinel structure. After 240 cycles, no traces of layered $LiM'O_2$ phase are observed near the surface (Fig. 6c) or in the bulk of NCM-00. Instead, strongspinel-like diffractions are shown along the $[10\bar{1}]$ zone axis of the bulk region (Fig. 6d). Fast Fourier transformation (FFT) to the HRTEM image within the square (inset of Fig. 6c) result in a pattern that is identical to the SAED pattern of the bulk region (Fig. 6d). Therefore, it is believed that the lithium-rich layered structure of NCM-00 is transformed to a spinel-like structure after 240 cycles. This agrees well with our CV plots and the previous reports. [10,43]

In contrast, the microstructure of NCM-10 after 240 cycles is complicated (Fig. 6e). FFT to the HRTEM image (inset of Fig. 6e) demonstrates the O3 diffractions (Square 2) and slightly stronger spinel-like diffractions (Square 1). In addition, the SAED pattern collected along the zone axis of the bulk (Fig. 6f) is an overlap of that of the

fundamental O3, cation-ordering of the Li_2MnO_3-like phase (marked with arrows), and weak spinel-like diffractions (marked with a triangle). These observations are well-reproducible, therefore, should be reliable. The discrepancy between the XRD and the SAED (Fig. 6) may be attributed to the low intensity of the cation ordering in the XRD patterns. Clearly, integration of spinel $LiNi_{0.5}Mn_{1.5}O_4$ suppresses the layer-to-spinel transition and stabilizes the structure of $Li_{1.2}Ni_{0.13}Co_{0.13}Mn_{0.54}O_2$, consistent with the results of Li-rich materials cycled at lower voltage (below 4.5V).[10]

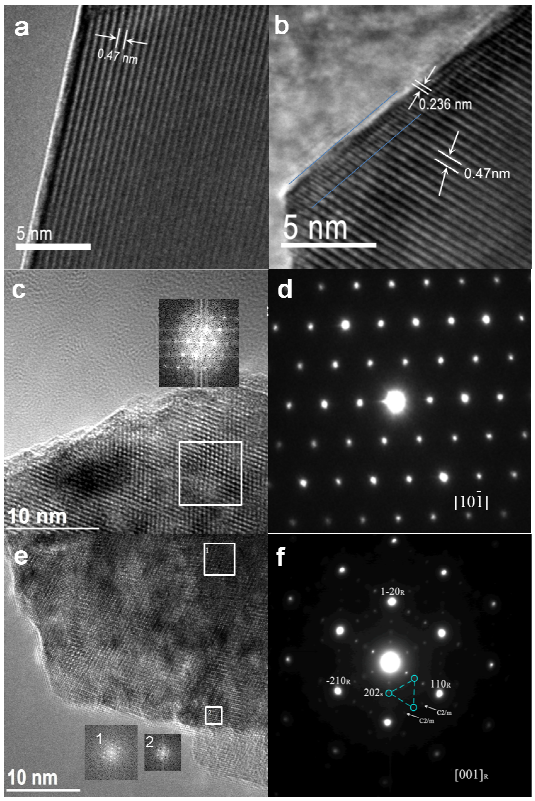

Fig. 6. HRTEM images of NCM-00 and NCM-10 before cycling (a,b), HRTEM and SAED images of NCM-00 (c,d) and NCM-10 (e,f) after 240 cycles.

Fig. 7 shows the proposed mechanism of improved electrochemical performance of LNMO-integrated Li-rich materials. According to the analysis of XRD, TEM, and electrochemical testing, cation migration occurs between $LiNi_{0.5}Mn_{1.5}O_4$ and $Li_{1.2}Ni_{0.13}Co_{0.13}Mn_{0.54}O_2$ during the calcination process, leading to the formation of a thin interface between $LiNi_{0.5}Mn_{1.5}O_4$ and $Li_{1.2}Ni_{0.13}Co_{0.13}Mn_{0.54}O_2$ due to long time sintering at high temperature. During the cycling process, the migration of cations between them caused the transformation from $LiNi_{0.5}Mn_{1.5}O_4$ to a new spinel phase S1, which largely suppressed the formation of the common spinel phase S2 ($LiMn_2O_4$-like) in the bulk of $Li_{1.2}Ni_{0.13}Co_{0.13}Mn_{0.54}O_2$, so the $LiNi_{0.5}Mn_{1.5}O_4$ that formed at the

surface of Li-rich material during sintering could stabilize the layered structure and improve the electrochemical performance.

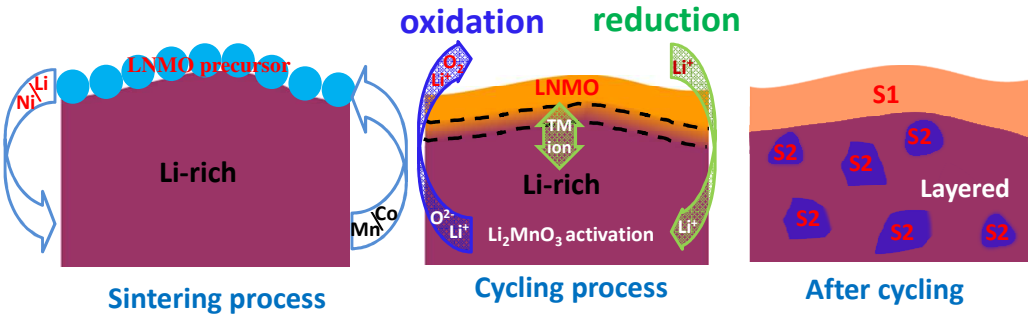

Fig. 7. Schematic of the proposed mechanism showing the migration of cations between $LiNi_{0.5}Mn_{1.5}O_4$ and $Li_{1.2}Ni_{0.13}Co_{0.13}Mn_{0.54}O_2$ during the calcination and the cycling process.

4. Conclusions

Integration of spinel $LiNi_{0.5}Mn_{1.5}O_4$ stabilizes the capacity and voltage of Li-rich layered $Li_{1.2}Mn_{0.54}Ni_{0.13}Co_{0.13}O_2$. Migration of cations occurs between integrated $LiNi_{0.5}Mn_{1.5}O_4$ spinel and $Li_{1.2}Mn_{0.54}Ni_{0.13}Co_{0.13}O_2$ during integration process. Although most of the $Li_{1.2}Mn_{0.54}Ni_{0.13}Co_{0.13}O_2$ degrades to new layered $LiM'O_2$ and $LiMn_2O_4$-like spinel by migration of the transition metal ions after long-term cycling, spinel $LiNi_{0.5}Mn_{1.5}O_4$ integration helps to suppress such degradation and that the integrated $LiNi_{0.5}Mn_{1.5}O_4$, like a seed of crystal growth, "absorbs" the cations that would otherwise form $LiMn_2O_4$-like phase. The preservation of the Li-rich layered structure and suppressed growth of $LiMn_2O_4$-like phase are believed to be responsible for the stabilized capacity and discharge voltage of the cathode material. These findings demonstrate a new way to improve the performances of the Li-rich Mn-based layered cathode materials.

Acknowledgement

This work was financially supported by the National Natural Science Foundation of China (NSFC No. 51372268).

Notes and references

a Institute of Physics, Chinese Academy of Sciences, P O Box 603, Beijing 100190, China. Fax: +86-10-82649046; Tel: +86-10-82649050; E-mail: zxwang@aphy.iphy.ac.cn

b X-ray Science Division, Argonne National Laboratory, 9700 South Cass Avenue, Argonne, Illinois 60439, United States

† Electronic Supplementary Information (ESI) available: details of dQ/dV and EELS of integrated samples and pristine sample. Supporting Information See DOI: 10.1039/b000000x

1 X. P. Gao and H. X. Yang, *Energy Environ. Sci.,* 2010, **3**, 174.

2 B. Xu, C. R. Fell, M. Chi and Y. S. Meng, *Energy Environ. Sci.,* 2011, **4**, 2223.

3 A. Boulineau, L. Simonin, J. F. Colin, C. Bourbon and S. Patoux, *Nano Lett.,* 2013, **13**, 3857.

4 L. Simonin, J. F. Colin, V. Ranieri, E. Canevet, J. F. Martin, C. Bourbon, C. Baehtz, P. Strobel, L. Daniel and S. Patoux, *J. Mater. Chem.,* 2012, **22**, 11316.

5 N. Yabuuchi, K. Yoshii, S. T. Myung, I. Nakai and S. Komaba, *J. Am. Chem. Soc.,* 2011, **133**, 4404.

6 A. Boulineau, L. Simonin, J. F. Colin, E. Canévet, L. Daniel and S. Patoux, *Chem. Mater.,* **2012**, **24,** 3558.

7 B. Song, Z. Liu, M. O. Lai and L. Lu, *Phys. Chem. Chem. Phys.,* 2012, **14**, 12875.

8 M. Gu, I. Belharouak, J. M. Zheng, H. M. Wu, J. Xiao, A. Genc, K. Amine, S. Thevuthasan, D. R. Baer, J. G. Zhang, N. D. Browning, J. Liu and C. M. Wang, *ACS Nano,* 2013, **7**, 760.

9 J. M. Zheng, M. Gu, J. Xiao, P. J. Zuo, C. M. Wang and J. G. Zhang, *Nano Lett.,* 2013, **13,** 3824.

10 D. Mohanty, A. S. Sefat, J. L. Li, R. A. Meisner, A. J. Rondinone, E. A. Payzant, D. P. Abraham, D. L. Wood III and C. Daniel, *Phys. Chem. Chem. Phys.,* 2013, **15**, 19496.

11 B. Song, M. O. Lai and L. Lu, *Electrochim. Acta,* 2012, **80**, 187.

12 Z. Q. Deng and A. Manthiram, *J. Phys. Chem. C,* 2011, **115**, 7097.

13 G. Singh, R. Thomas, A. Kumar and R. S. Katiyar, *J. Electrochem. Soc.,* 2012, **159**, A410.

14 K. R. Chemelewski, D. W. Shin, W. Li and A. Manthiram, *J. Mater. Chem. A*, 2013, **1**, 3347.

15 S. H. Kang and K. Amine, *J. Power Sources,* 2005, **146**, 654.

16 G. R. Li, X. Feng, Y. Ding, S. H. Ye and X. P. Gao, *Electrochim. Acta,* 2012, **78**, 308.

17 Q. Q. Qiao, H. Z. Zhang, G. R. Li, S. H. Ye, C. W. Wang and X. P. Gao, *J. Mater. Chem. A,* 2013, **1**, 5262.

18 X. F. Zhang, I. Belharouak, L. Li, Y. Lei, J. W. Elam, A. Nie, X. Q. Chen, R. S. Yassar and R. L. Axelbaum, *Adv. Energy Mater.,* 2013, **3**, 1299.

19 C. R. Wu, X. P. Fang, X. W. Guo, Y. Mao, J. Ma, C. C. Zhao, Z. X. Wang and L. Q. Chen, *J. Power Sources,* 2013, **231**, 44.

20 H. Z. Zhang, Q. Q. Qiao, G. R. Li and X. P. Gao, *J. Mater. Chem. A*, 2014, **2**, 7454.

21 B Li, H J Yan, J Ma, P R Yu, D G Xia, W F Huang,W S Chu and Z Y Wu, *Adv. Funct. Mater.,* 2014, DOI: 10.1002/adfm.201400436.

22 H F Li, J Pang, Y P Yin, W D Zhuang, H Wang, C X Zhai and S G Lu, *RSC Adv.*,2013, **3**,13907.

23 K. R. Chemelewski and A. Manthiram, *J. Phys. Chem. C,* 2013, **117**, 12465.

24 M. M. Thackeray, C. S. Johnson, J. T. Vaughey, N. Li and S. A. Hackney, *J. Mater. Chem.,* 2005, **15**, 2257.

25 S. H. Park, S. H. Kang, C. S. Johnson, K. Amine and M. M. Thackeray, *Electrochem. Commun.,* 2007, **9**, 262.

26 C. S. Johnson, N. Li, J. T. Vaughey, S. A. Hackney and M. M. Thackeray, *Electrochem. Commun.,* 2005, **7**, 528.

27 Z. H. Lu, L. Y. Beaulieu, R. A. Donaberger, C. L. Thomas and J. R. Dahn, *J. Electrochem. Soc.,* 2002, **149**, A778.

28 T. Ohzuku, M. Nagayama, K. Tsuji and K. Ariyoshi, *J. Mater. Chem.,* 2011, **21**, 10179.

29 J. H. Kim, S. T. Myung, C. S. Yoon, S. G. Kang and Y. K. Sun, *Chem. Mater.,* 2004, **16**, 906.

30 A. R. Armstrong, M. Holzapfel, P. Novák, C. S. Johnson, S. H. Kang, M. M. Thackeray and P. G. Bruce, *J. Am. Chem. Soc.,* 2006, **126**, 8694.

31 K. Ariyoshi, Y. Iwakoshi, N. Nakayama and T. Ohzuku, *J. Electrochem. Soc.,* 2004, **151**, A296.

32 S. H. Park, S. W. Oh, S. H. Kang, I. Belharouak, K. Amine and Y. K. Sun, *Electrochim. Acta,* 2007, **52**, 7226.

33 C. S. Johnson, N. C. Li, C. Lefief, J. T. Vaughey and M. M. Thackeray, *Chem. Mater.,* 2008, **20**, 6095.

34 X. Q. Yu, Y. C Lyu, L. Gu, H. M. Wu, S. M. Bak, Y. N. Zhou, K. Amine, S. N. Ehrlich, H. Li, K. W. Nam and X. Q. Yang, *Adv. Energy Mater.,* 2014, **4**, 1300950

35 C. Ghanty, R. N. Basu and S.B. Majumder, *Solid State Ionics,* 2014, **256**, 19

36 H. H. Li, N. Yabuuchi, Y. S. Meng, S. Kumar, J. Breger, C. P. Grey and Y. S. Horn, *Chem. Mater.,* 2007, **19**, 2551.

37 J. Bre, Y. S. Meng, Y. Hinuma, S. Kumar, K. Kang, G. C. Y. S. Horn and C. P. Grey, *Chem. Mater.,* 2006, **18**, 4768.

38 S. H. Kang, C. S. Johnson, J. T. Vaughey, K. Amine and M. M. Thackeray, *J. Electrochem. Soc.,* 2006, **153**, A1186.

39 B. Song, H. W. Liu, Z. W. Liu, P. F. Xiao, M. O. Lai and L. Lu, *Sci. Rep.,* 2013, **3**, 3094.

40 C. S. Johnson, N. C. Li, C. Lefief, J. T. Vaughey and M. M. Thackeray, *Chem. Mater.,* 2008, **20**, 6095.

41 M. W. Jang, H. G. Jung, B. Scrosati and Y. K. Sun, *J. Power Sources,* 2012, **220**, 354.

42 C. Zhan, J. Lu, A. J. Kropf, T. P. Wu, A. N. Jansen, Y. K. Sun, X. P. Qiu and K. Amine, *Nat. Commun.,* 2013, **4**, 2437.

43 D. Mohanty, A. S. Sefat, S. Kalnaus, J. L. Li, R. A. Meisner, E. A. Payzant, D. P. Abraham, D. L. Wood and C. Daniel, J. Mater. Chem. A, 2013, 1, 6249.